The 0p shell revisited

R. E. Julies
Physics Department, University of the Western Cape, Private Bag X17, Bellville, C.P. 7530, Republic of South Africa

W. A. Richter
Physics Department, University of Stellenbosch, Stellenbosch 7600, Republic of South Africa

B. A. Brown
National Superconducting Cyclotron Laboratory and Department of Physics and Astronomy, Michigan State University East Lansing, MI, 48824 United States of America

Received: 15 June 1992

New effective interactions for the 0p shell are obtained from fits to parameters of a potential model as well as two-body matrix elements. An updated set of ground-state binding and excitation energies (77 versus the approximately 40 energy levels of specified (J,T) of Cohen and Kurath) of the natural parity states in A = 5–16 nuclei has been used. Improved wavefunctions which reproduce the energy levels within an rms deviation of about 550 keV are obtained by including a mass-dependence of $A^{-0.17}$ for the two-body matrix elements. The effect of mass-dependent single-particle energies are also considered and the relative importance of the antisymmetric spin-orbit interaction is investigated. Comprehensive calculations of M1 and E2 moments and transition strengths, log ft values and Gamow-Teller strength distributions have been carried out. Good agreement between experimental values and the calculated observables is generally found. It is concluded that there appears to be no particular advantage in fitting the parameters of the interaction to static moments as well as energies.

Nuwe effektiewe wisselwerkings vir die 0p-skil is verkry vanaf passings aan parameters van 'n potensiaalmodel sowel as tweedeeltjiematrikselemente. 'n Bygewerkte stel grondtoestandbindings- en opwekkings-energieë (77 teenoor die ongeveer 40 energievlakke van bepaalde (J,T) van Cohen en Kurath) van die natuurlike pariteitstoestande in A =5-16 kerne is gebruik. Verbeterde golffunksies wat die energievlakke binne 'n wgk afwyking van 550 keV reproduseer is verkry deur massa-afhanklikheid van $A^{-0.17}$ vir die tweedeeltjiematrikselemente in te sluit. Die effek van massa-afhanklike enkeldeeltjie-energieë is ook ondersoek asook die relatiewe belangrikheid van die antisimmetriese spin-orbitale wisselwerking. Omvattende berekenings van M1 en E2 momente en oorgangssterktes, log ft waardes en Gamov-Teller sterkteverdelings is uitgevoer. Goeie ooreenstemming tussen eksperimentele waardes en berekende waarneembares is in die algemeen verkry. Daar word ook tot die gevolgtrekking gekom dat daar geen bepaalde voordeel blyk te wees in die passing van parameters van die wisselwerking aan statiese momente sowel as energieë nie.

1 Introduction

The 0p shell has traditionally served as a 'test' for nuclear models since early studies of nuclear structure. Many shell-model calculations on light nuclei with A = 4–16 have been carried out (see refs. [1] to [17]). The most well-known calculations are those of Cohen and Kurath [6], who obtained their matrix elements by (a) using the so-called TBME or model-independent (MI) methods in which the 15 two-body matrix elements and 2 single-particle energies are treated as adjustable parameters in fits to selected sets of experimental binding energies of natural-parity states in A = 6(8)–16 nuclei and (b) using a 13-parameter potential model in the LS representation. The two model-independent interactions are referred to in the literature as the 2BME(6–16) and 2BME(8–16) interactions respectively, and the interaction obtained from their potential model parameterization as CKPOT.

It has also been shown that some simple interaction forms, such as the modified surface delta interaction (MSDI), yield results in the 0p shell that are comparable to those obtained by Cohen and Kurath (see refs. [8] and [10] to [13]).

More complex shell-model calculations involving these nuclei have also been carried out. Examples are the spurious-free shell-model calculations of van Hees *et al* [16] in a complete $(0+1)\hbar\omega$ model space, the shell-model calculations of Irvine *et al* [18] in which multi-particle excitations (up to $6\hbar\omega$) from the 0p to the 1s0d shell are included, and the calculations of the Utrecht group [17] who obtained their interactions by fitting simultaneously to energies as well as static electromagnetic moments.

The effective interaction may also be derived via the G–matrix method. Hauge and Maripuu [9] have applied the effective Sussex potential of Elliot *et al* [19, 20] in their 0p shell calculations in which (1) the energy separation between the $p_{\frac{3}{2}}$ and $p_{\frac{1}{2}}$ single-particle states, and (2) the harmonic-oscillator size parameter were allowed to vary. Their results show that the former parameter greatly affects the calculated levels and that the size parameter, to a good approximation, can be treated as a constant (1.7 fm) over the mass range considered. It was shown by Yoro [14] that the Cohen-Kurath and Hauge-Maripuu interactions are very similar although basically different methods were followed in determining them. The most striking difference between the interactions of Cohen and

ently in the two cases, being mainly in the one-body part for Hauge-Maripuu, and mainly in the two-body part for Cohen-Kurath, the results are quite similar.

The $0p$ shell is particularly suited for detailed microscopic analyses because of the vast wealth of spectroscopic data available for this shell and the relatively small number of single-particle orbits required for describing the configurations, if compared to the $1s0d$ or $0f1p$ shells. As much more experimental information on these nuclei are now available we extend some of the earlier calculations by fitting to a new expanded set of data. The new sets of wave functions obtained from our fits are utilized in the calculation of observables which are primarily dependent on the $0p$ shell nature of the states e.g. static electromagnetic moments, electromagnetic transition strengths, and Gamow-Teller strengths.

Only shell-model calculations on natural-parity states were carried out, i.e. states with parity $(-1)^A$. For shell-model calculations involving unnatural parity states the reader is referred to refs. [21, 22, 23, 13] and [16]. We have carried out both model-independent and potential model parameterization fits in the $0p$ shell. The interaction obtained from model-independent fits in which the 15 two-body matrix elements and two single-particle energies were treated as free parameters is the equivalent of the 2BME(6-16) interaction of Cohen and Kurath, except that an extended and updated data set (with the inclusion of $A = 5$) is used and refinements such as a mass dependence of the two-body matrix elements are incorporated (see section 3).

In section 2 a breakdown is given of the experimental data that was used in the iteration procedure (see ref [24] for details of the procedure) for determining the parameter values. The results of the fits to the selected set of experimental energies are presented in section 3. The two-body matrix elements of various interactions for the $0p$ shell, including those obtained from our fits, are compared in the spin-tensor decomposition plots of the interactions presented in section 4. In section 5 the static electromagnetic moments and transition strengths of $0p$-shell nuclei are calculated and compared with experiment and also other shell-model calculations. The log ft values and Gamow-Teller strength distributions are compared with experiment, and presented in section 6. The final remarks regarding the $0p$ shell are made in the concluding section.

2 Data selection

Our calculations were performed in the complete $0\hbar\omega$ model space, using a set of experimental data for nuclei with mass numbers $A = 5$–16, with the ^{4}He nucleus taken as the core. Only states with configurations of the form $(0p)^{A-4}$ were included in the calculations. Care was also taken to exclude all intruder states as well as states with uncertain or ambiguous spin-isospin assignments. Our chosen set of 77 experimental ground-state and excitation energies (compared to about 40 used by Cohen and Kurath [6]), taken from refs. [25] to [29], is listed in Table 1.

A charge-independent Hamiltonian was used in the calculations which were done in the isospin formalism. The iterative fitting procedure could only be carried out once the Coulomb contribution to the total energy had been removed from the experimental binding energies. (The iteration procedure is outlined in detail in ref. [24] and will not be repeated here.) Various methods for estimating the Coulomb contribution have been described in the literature (see, for example ref. [30]). Where possible, the estimates were obtained by taking the difference between the binding energies of pairs of analogue states, one generally being a ground state. Where the above method could not be applied the Coulomb contributions were estimated from a graph of displacement energy versus A. Table 2 contains a list of our Coulomb estimates, which are compared to those used by Cohen and Kurath for

Table 2 List of Coulomb-corrected Binding Energies

Nucleus	A	BE[a] (relative to ^{4}He)	Coulomb contribution CK[b]	Coulomb contribution present	Coulomb-corrected BE
He	5	0.8859	—	0.000	0.886
Li	6	-3.6997	1.00	0.83[c]	-4.53
Li	7	-10.9498	1.00	0.82[d]	-11.77
Li	8	-12.9826	—	0.95[e]	-13.93
Be	8	-28.2040	2.64	2.45[e]	-30.66
Be	9	-29.8694	2.64	2.40	-32.27
Be	10	-36.6814	—	2.20	-38.88
B	10	-36.4553	4.61	4.24	-40.70
Li	11	-17.2441	—	0.76	-18.00
B	11	-47.9095	4.61	4.13	-52.04
C	12	-63.8665	7.23	6.67	-70.54
C	13	-68.8129	7.23	6.58	-75.39
N	14	-76.3635	10.24	10.05	-86.41
N	15	-87.1968	—	10.34	-97.54
O	16	-99.3243	13.83	13.83	-113.16

[a] Calculated from data in refs. [31], [25-29].

[b] CK denotes the calculations of Cohen and Kurath.

[c] Calculated from the binding energy difference between the $0^+, 1$ analogue states in $A = 6$ nuclei.

[d] Calculated from the binding energy difference between the $\frac{3}{2}^-, \frac{3}{2}$ analogue states in $A = 7$ nuclei.

[e] Calculated from the binding energy difference between the $0^+, 2$ analogue states in $A = 8$ nuclei.

Table 4 Parameter values for the PNOALS interaction with $P = 0.17$ for the TBME mass dependence

Component	S	T	Form	Range (fm)	Parameter value[a] (MeV)	Error (MeV)
Two-body parameters						
Central	0	0	DI-HSM3	0.20, 0.33, 0.50	-0.8229	0.41
			DI-FOPEP	1.414	1.000	
	1	0	DI-HSM3	0.20, 0.33, 0.50	0.8183	0.02
			DI-FOPEP	1.414	1.000	
			C		-0.8330	0.16
	0	1	DI-HSM3	0.20, 0.33, 0.50	1.912	0.05
			DI-FOPEP	1.414	1.000	
			C		2.921	0.16
	1	1	DI-HSM3	0.20, 0.33, 0.50	-1.411	0.35
			DI-FOPEP	1.414	1.000	
Tensor	1	0	DI-S	0.25	-1.794	0.23
			DI-OPEP	1.414	-0.5090	0.06
	1	1	DI-S	0.25	2.301	0.24
			DI-FOPEP	1.414	1.000	
Spin-orbit	1	0	DI-S	0.25	5.175	0.78
	1	1	DI-S	0.25	0.9189	0.13
Single-particle parameters						
SPE($A = 5$)				$0p_{\frac{1}{2}}$	4.404	0.10
				$0p_{\frac{3}{2}}$	2.096	0.04
SPE($A = 15$)-SPE($A = 5$)				$0p_{\frac{1}{2}}$	0.2859	0.05
				$0p_{\frac{3}{2}}$	0.0832	0.05

[a] A value of 1 implies that the strength parameters $(SP)_i$ in eq. (13) of ref. [24] have the values corresponding to the bare G−matrix of Hosaka, Kubo and Toki [32].

3. a two-parameter spin-orbit component containing for each (S,T) channel

   (a) a single short-ranged OBEP term, and

4. zero for the ALS component.

The parameter values for the PNOALS interaction are listed in Table 4 and those for the the PTBME interaction in Table 5.

The 6 independent parameters for the central component are made up as follows: two for the $(S,T) = (0,1)$ and $(S,T) = (1,0)$ and one each for the $(S,T) = (0,0)$ and $(S,T) = (1,1)$ channels (see Fig. 13). We have decided to vary all the range terms of this component thereby restricting the monopole terms only to the $(S,T) = (0,1)$ and $(1,0)$ channels.

The inclusion of a mass-dependence for the two-body matrix elements and single-particle energies as well as a density-dependence of the interaction has led to improved fits for the $1s0d$ and $0f1p$ shells (see refs. [24, 33]). We now examine the dependencies of the PTBME and PNOALS interactions upon these quantities.

3.3.1 Mass dependence of the TBME

As in the case of the $1s0d$ shell, the mass-dependence of the two-body matrix elements was assumed to be of the

Table 5 Parameter values of the PTBME interaction with $P = 0.17$ for the two-body matrix elements and mass-independent SPE

$2j_a$	$2j_b$	$2j_c$	$2j_d$	JT	$< j_a j_b \lvert V \rvert j_c j_d >_{JT}$ (MeV)
Two-body parameters					
1	1	1	1	10	-3.5383
1	1	1	1	01	-0.6188
1	1	3	1	10	2.0001
1	1	3	3	10	2.6524
1	1	3	3	01	-4.1265
3	1	3	1	10	-6.0149
3	1	3	1	20	-5.0237
3	1	3	1	11	~~-4.5526~~
3	1	3	1	21	~~-1.6697~~
3	1	3	3	10	4.0113
3	1	3	3	21	-1.6633
3	3	3	3	10	-3.3558
3	3	3	3	30	-5.8166
3	3	3	3	01	-3.2533
3	3	3	3	21	-0.9119
Single-particle parameters					
SPE($A = 5$)				$0p_{\frac{1}{2}}$	4.3522
				$0p_{\frac{3}{2}}$	2.1422

0.7552

The spectrum of ^{8}Be. Only the $T = 0$ levels in this nucleus were used in the fit. The higher-lying levels (above 11 MeV) calculated from PNOALS and PTBME lie much closer to the experimental levels than those calculated with the CKPOT interaction.

The spectrum of ^{9}Be. Our calculated spectra generally lie closer to the experimental spectrum than the CKPOT case, with the first $\frac{5}{2}^-, \frac{1}{2}$ and $\frac{1}{2}^-, \frac{1}{2}$ levels reproduced in the correct order, in contrast to CKPOT. It should be remarked here that the $\frac{5}{2}^-$-assignment for the 7.94 MeV level as suggested by the β-decay work of D. Mikolas *et al* [34] and supported by the shell-model calculations of Cohen and Kurath, was adopted for our energy fits.

The spectrum of ^{10}Be. The first and second excited $2^+, 1$ states are reproduced too low by about 2 MeV by the CKPOT interaction. Good correspondence with the experimental spectrum is found for these levels, and also the ground state, for both the PNOALS and PTBME interactions. The experimental $0^+, 1$ state at 6.179 MeV for which no shell-model counterpart exists, is considered to be an intruder state (see also ref. [16]).

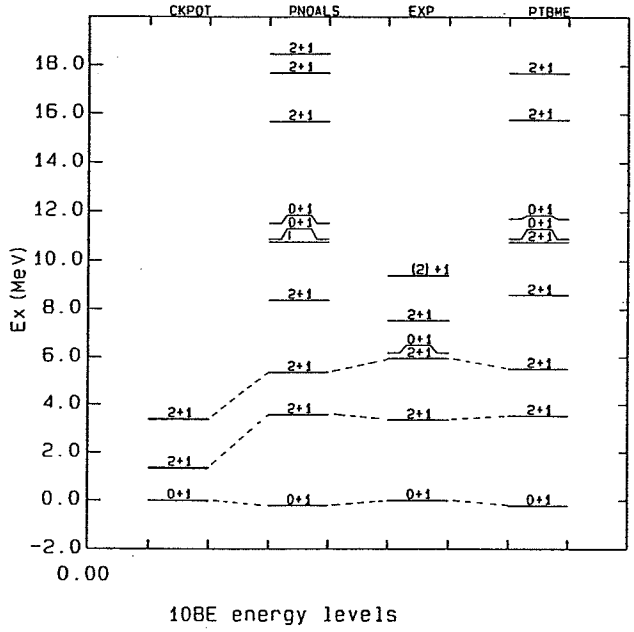

Figure 6 Energy levels in ^{10}Be. The conventions are the same as in Fig. 1.

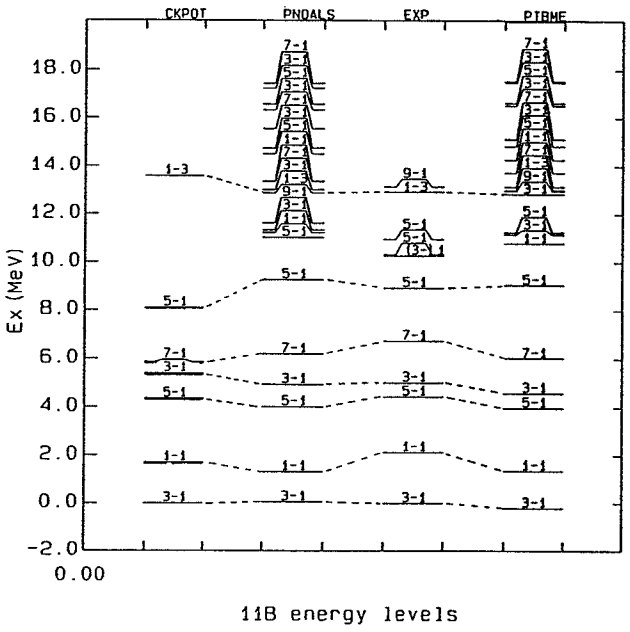

Figure 8 Energy levels of ^{11}B. The conventions are the same as in Fig. 1.

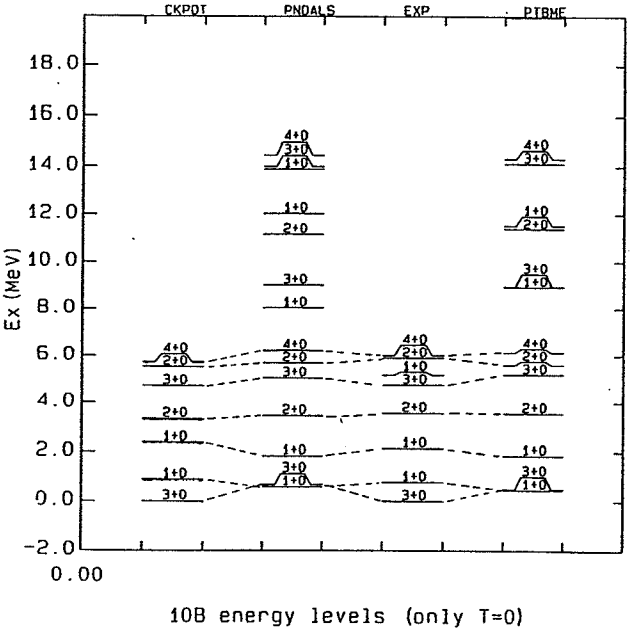

Figure 7 Energy levels of ^{10}B. The conventions are the same as in Fig. 1.

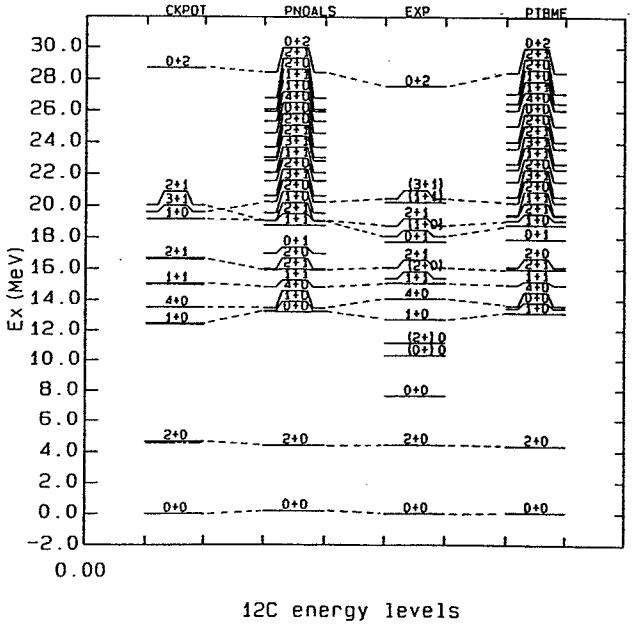

Figure 9 Energy levels of ^{12}C. The conventions are the same as in Fig. 1.

The spectrum of ^{10}B. Except for a virtual degeneracy for the ground- and first excited state for both the PNOALS and PTBME cases our calculated spectra agree quite well with experiment. The level ordering for the known remaining low-lying states is correctly reproduced by our interactions as well as the CKPOT interaction. The observed $1^+, 0$ level at 5.18 MeV was not included in the energy fit because of the experimental evidence that the configuration is not p^6 (see ref. [10]).

The spectrum of ^{11}B. Compared to the CKPOT case the agreement with experiment is marginally better, with our calculated ground-state energies lying close to the experimental one. The first $T = \frac{3}{2}$ level was included in the fit.

The spectrum of ^{12}C. Very good agreement between theory and experiment is achieved. The reversal of the second 2^+, 1, and 3^+, 1 states in the CKPOT calculation is corrected. The ground-state energies correspond exceptionally well. The states observed between 6 and 12 MeV are assumed to be intruders [16] and are therefore not reproduced.

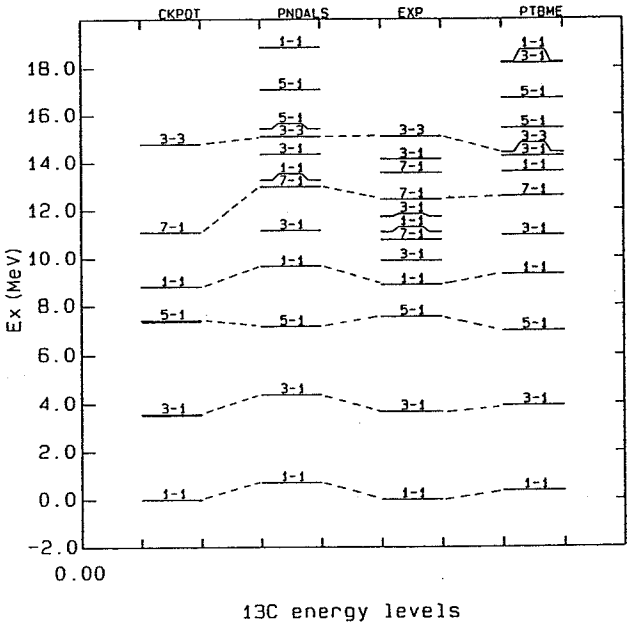

Figure 10 Energy levels of ^{13}C. The conventions are the same as in Fig. 1.

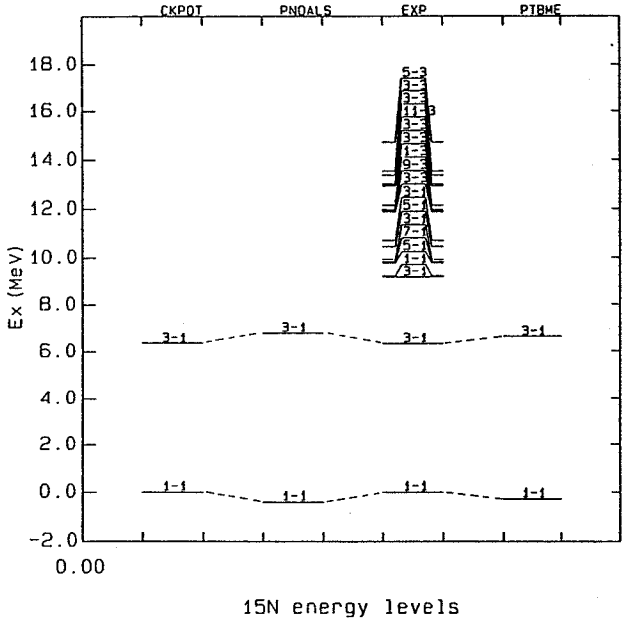

Figure 12 Energy levels of ^{15}N. The conventions are the same as in Fig. 1

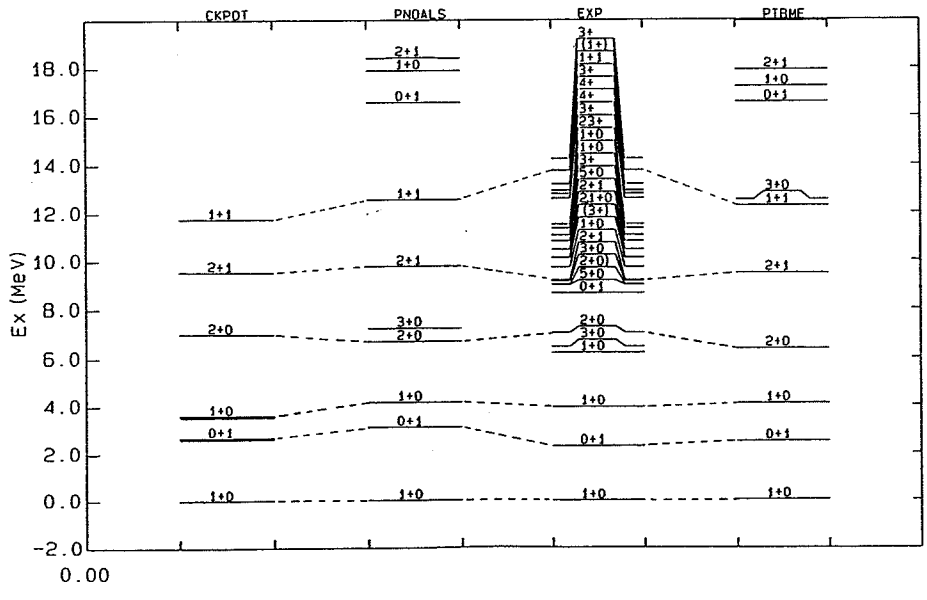

Figure 11 Energy levels of ^{14}N. The conventions are the same as in Fig. 1.

moments and transition rates with experiment therefore provide a much more sensitive test for the calculated wave functions than the calculated energy spectrum.

5.1 Magnetic dipole moments

As a means of 'testing' the wave functions the magnetic dipole moments for the (normal-parity) ground states of $A = 6 - 15$ nuclei, using both the PNOALS and PTBME interactions, have been calculated. Use was made of effective $g-$factors obtained from a least-squares fit to the experimental magnetic dipole moments. The fitted $g-$factors for both the PNOALS and PTBME interactions are compared with the bare $g-$factors in Table 7.

Our results are compared with their experimental counterparts (taken from refs.[26] to [29]) in Table 8.

Apart from a few exceptions the present calculations reproduce the experimental values very well, with the PTBME interaction doing slightly better than the PNOALS interaction. The results obtained by Cohen and Kurath [6] with the CKPOT interaction, and the calculations of Van Hees *et al* [17], labelled by CKPOT and vHGW respectively in Table 8, are shown for comparison. It should be mentioned that the empirical vHGW interaction [17] used for the calculation of these dipole moments was obtained by fitting to energy spectra as well as magnetic dipole and quadrupole moments, giving rise to a very low rms deviation of 0.062 μ_N (compared to the 0.129 μ_N for the CKPOT interaction, see Table 9) between experiment and theory for the dipole moments.

The agreement of the vHGW results with experiment is very similar to that of our interactions. (Each of our values that does better than vHGW in Table 8 is underlined.) The rms deviations for the dipole and quadrupole moments are compared in Table 9. The values for the (8–16)CKPOT interaction are also shown. The PTBME and vHGW interactions are almost equally good in reproducing the magnetic dipole moments. The results suggest that there is no particular advantage to fitting static moments along with the energies, rather than fitting only the energies and determining optimum effective $g-$factors afterwards. In fact our rms deviations for energies (of the natural parity states) are somewhat smaller than the corresponding vHGW values [17].

Table 7 Comparison between the bare and fitted $g-$factors

				Present results	
	Bare nucleon value	(8–16)CKPOT	vHGW[a]	PTBME	PNOALS
g_s-proton	5.586	5.510	5.543	5.644	5.531
g_s-neutron	-3.826	-3.821	-3.875	-3.994	-4.012
g_l-proton	1.000	1.058	1.030	1.109	1.138
g_l-neutron	0.000	-0.013	0.036	-0.049	-0.007

[a] vHWG denotes the interaction of van Hees *et al* [17].

Table 8 Magnetic dipole moments (in units of μ_N) of natural parity $A = 6-15$ nuclei (using the fitted $g-$factors listed in Table 7)

Nucleus	J^π	experiment[a]	CKPOT	vHGW[b]	PTBME	PNOALS
^{6}Li	1^+	0.822	0.864	0.864	0.815[c]	0.757
^{7}Li	$\frac{3}{2}^-$	3.256	3.261	3.273	3.247	3.223
^{8}Li	2^+	1.653	1.366	1.612	1.442	1.207
^{8}Be	2^+	1.036	1.298	1.019	1.044	1.134
^{9}Li[d]	$\frac{3}{2}^-$	3.439	3.483	3.430	3.435	3.398
^{9}Be	$\frac{3}{2}^-$	-1.178	-1.244	-1.070	−1.199	−1.163
^{10}B	3^+	1.801	1.811	1.854	1.823	1.864
	1^+	0.63 ± 0.124	0.800	0.804	0.733	0.733
^{11}B	$\frac{3}{2}^-$	2.689	2.630	2.723	2.686	2.673
^{11}C	$\frac{3}{2}^-$	-0.964	-0.889	-0.924	−0.933	-0.855
^{12}B	1^+	1.003	0.760	0.899	0.820	0.870
^{12}N	1^+	0.457	0.613	0.470	0.539	0.459
^{13}B	$\frac{3}{2}^-$	3.178	3.151	3.208	3.245	3.244
^{13}C	$\frac{1}{2}^-$	0.702	0.757	0.753	0.751	0.809
^{13}N	$\frac{1}{2}^-$	-0.322	-0.384	-0.324	-0.340	-0.309
^{14}N	1^+	0.404	0.331	0.394	0.375	0.480
^{15}N	$\frac{1}{2}^-$	-0.283	-0.264	-0.238	-0.216	-0.163
^{15}O	$\frac{1}{2}^-$	0.719	0.638	0.670	0.633	0.664

[a] See refs. [26-29].

[b] vHGW denotes the interaction of van Hees *et al* [17].

[c] See text for meaning of underlining.

[d] not included in the energy fits.

Table 11 Magnetic dipole transitions in $0p$–shell nuclei calculated with the g–factors listed in Table 7

Nucleus	E_{x_i} (MeV)	→	E_{x_f} (MeV)	J_i^π	→	J_f^π [a]	$B(\mu_N^2)$ Exp.[b]	HM[c]	PTBME
^{6}Li	3.56	→	0	$0^+;1$	→	$1^+;0$	15.4 ± 0.3	16.4	17.6
	5.37	→	0	$2^+;1$	→	$1^+;0$	0.15 ± 0.03	0.00760	0.025
^{7}Li	0.48	→	0	$\frac{1}{2}^-$	→	$\frac{3}{2}^-$	4.92 ± 0.25	4.42	4.62
^{8}Li	0.98	→	0	1^+	→	2^+	5.0 ± 1.6	5.06	4.87
	2.26	→	0	3^+	→	2^+	0.52 ± 0.02	0.578	0.614
^{8}Be	17.64	→	3.04	$1^+;1$	→	$2^+;0$	0.218 ± 0.002	0.00885	0.055
	18.15	→	0	$1^+;0$	→	$0^+;0$	0.043	0.00087	0.0037
		→	3.04		→	$2^+;0$	0.091	0.00052	0.0001
	19.07	→	3.04	$3^+;(1)$	→	$2^+;0$	0.2		0.102
	27.49	→	17.64	$0^+;2$	→	$1^+;1$	2.0 ± 0.4		2.49
^{8}B	0.78	→	0	1^+	→	2^+	9.1 ± 4.5	3.97	3.98
^{9}Be	2.43	→	0	$\frac{5}{2}^-$	→	$\frac{3}{2}^-$	0.54 ± 0.05	0.422	0.553
	14.39	→	0	$\frac{3}{2}^-;\frac{3}{2}$	→	$\frac{3}{2}^-;\frac{1}{2}$	0.20 ± 0.02	0.111	0.246
		→	2.43		→	$\frac{5}{2}^-;\frac{1}{2}$	0.39 ± 0.05	0.310	0.481
	16.98	→	0	$\frac{1}{2}^-;\frac{3}{2}$	→	$\frac{3}{2}^-;\frac{1}{2}$	0.288 ± 0.021		0.249
		→	2.78		→	$\frac{1}{2}^-;\frac{1}{2}$	0.07 ± 0.02		0.0319
^{10}B	1.74	→	0.72	$0^+;1$	→	$1^+;0$	> 2	6.27	14.7
	2.15	→	0.72	$1^+;0$	→	$1^+;0$	0.0025 ± 0.0004	0.0193	0.0115
		→	1.74		→	$0^+;1$	0.20 ± 0.02	2.46	0.279
	3.59	→	0	2^+	→	3^+	0.0015 ± 0.0003	0.0132	0.00274
		→	0.72		→	1^+	0.011 ± 0.001	0.0114	0.0021
		→	2.15		→	1^+	0.017 ± 0.0034	0.0053	0.0137
	4.77	→	0	3^+	→	3^+	0.000079 ± 0.000021	0.0201	0.000204
	5.16	→	0	$2^+;1$	→	$3^+;0$	0.041 ± 0.004	0.00078	0.0130
		→	0.72		→	$1^+;0$	0.32 ± 0.04	3.41	2.32
		→	3.59		→	$2^+;0$	2.5 ± 0.4	1.34	2.87
	5.92	→	0	2^+	→	3^+	0.050 ± 0.013		0.0191
		→	0.72		→	1^+	0.018 ± 0.005		0.0006
	6.03	→	0	4^+	→	3^+	0.042 ± 0.007		0.0031
^{11}B	2.13	→	0	$\frac{1}{2}^-$	→	$\frac{3}{2}^-$	1.1 ± 0.1	1.40	1.81
	4.45	→	0	$\frac{5}{2}^-$	→	$\frac{3}{2}^-$	0.54 ± 0.04	0.574	0.487
	5.02	→	0	$\frac{3}{2}^-$	→	$\frac{3}{2}^-$	1.13 ± 0.04	1.39	1.36
		→	2.13		→	$\frac{1}{2}^-$	0.98 ± 0.04	0.877	1.08
	6.74	→	4.45	$\frac{7}{2}^-$	→	$\frac{5}{2}^-$	0.0063 ± 0.0016	0.0390	0.0413
	8.56	→	0	$\frac{3}{2}^-$	→	$\frac{3}{2}^-$	0.071 ± 0.007	0.123	0.0001
		→	2.13		→	$\frac{1}{2}^-$	0.091 ± 0.009	0.351	0.125
		→	4.45		→	$\frac{5}{2}^-$	0.057 ± 0.01	0.604	0.133
		→	5.02		→	$\frac{3}{2}^-$	0.16 ± 0.023		0.022
	8.92	→	0	$\frac{5}{2}^-$	→	$\frac{3}{2}^-$	0.55 ± 0.04	0.604	0.377
		→	4.45		→	$\frac{5}{2}^-$	0.23 ± 0.02	0.0307	0.023
^{11}C	2.00	→	0	$\frac{1}{2}^-$	→	$\frac{3}{2}^-$	0.68 ± 0.05	0.888	1.32
	8.11	→	0	$\frac{3}{2}^-$	→	$\frac{3}{2}^-$	0.041 ± 0.009	0.188	0.0040
		→	2.00		→	$\frac{1}{2}^-$	0.034 ± 0.009	0.312	0.103
	8.42	→	0	$\frac{5}{2}^-$	→	$\frac{3}{2}^-$	0.45 ± 0.18	0.778	0.364
^{12}B	0.95	→	0	2^+	→	1^+	0.25 ± 0.04	0.194	0.230

Table 12 Electric quadrupole transitions in $0p$–shell nuclei using the effective charges listed in Table 7

Nucleus	E_{x_i} (MeV)	→	E_{x_f} (MeV)	J_i^π	→	J_f^π [a]	$B(e^2.fm^4)$ Exp. [b]	$B(e^2.fm^4)$ PTBME
^{6}Li	2.19	→	0	3^+	→	1^+	10.71 ± 0.84	3.51
	4.31	→	0	2^+	→	1^+	4.4 ± 2.3	2.92
^{7}Li	0.48	→	0	$\frac{1}{2}^-$	→	$\frac{3}{2}^-$	15.7 ± 1.0	9.19
	4.63	→	0	$\frac{7}{2}^-$	→	$\frac{3}{2}^-$	3.4	3.70
^{8}Be	17.64	→	3.04	1^+1	→	2^+0	0.27 ± 0.12	1.52
^{9}Be	2.43	→	0	$\frac{5}{2}^-$	→	$\frac{3}{2}^-$	27.2 ± 2.0	18.25
	6.76	→	0	$\frac{7}{2}^-$	→	$\frac{3}{2}^-$	7.0 ± 3.0	5.72
	16.98	→	2.43	$\frac{1}{2}^-;\frac{3}{2}$	→	$\frac{5}{2}^-;\frac{1}{2}$	1.0 ± 0.2	0.885
^{10}Be	3.37	→	0	2^+	→	0^+	10.25 ± 1.0	10.5
^{10}B	0.72	→	0	1^+	→	3^+	4.14 ± 0.06	1.90
	2.15	→	0	1^+	→	3^+	1.72 ± 0.26	4.90
		→	0.72		→	1^+	0.83 ± 0.40	5.05
	3.59	→	0	2^+	→	3^+	1.15 ± 0.38	1.71
	4.77	→	0.72	3^+	→	1^+	20 ± 3	8.61
	6.03	→	0	4^+	→	3^+	19 ± 3	11.31
^{10}C	3.35	→	0	2^+	→	0^+	12.3 ± 2.1	5.46
^{11}B	4.45	→	0	$\frac{5}{2}^-$	→	$\frac{3}{2}^-$	14.0 ± 3.5	14.2
	5.02	→	2.13	$\frac{3}{2}^-$	→	$\frac{1}{2}^-$	4.4 ± 2.9	3.05
	6.74	→	0	$\frac{7}{2}^-$	→	$\frac{3}{2}^-$	1.9 ± 0.44	2.90
	8.92	→	0	$\frac{5}{2}^-$	→	$\frac{3}{2}^-$	1.2 ± 0.58	0.02
^{12}C	4.44	→	0	2^+	→	0^+	7.60 ± 0.43	11.28
	16.11	→	0	$2^+;1$	→	$0^+;0$	0.65 ± 0.13	0.801
^{13}C	3.68	→	0	$\frac{3}{2}^-$	→	$\frac{1}{2}^-$	6.4 ± 1.5	9.66
	7.55	→	0	$\frac{5}{2}^-$	→	$\frac{1}{2}^-$	5.6 ± 0.4	9.42
	15.11	→	0	$\frac{3}{2}^-;\frac{3}{2}$	→	$\frac{1}{2}^-;\frac{1}{2}$	0.91 ± 0.18	1.14
^{13}N	3.51	→	0	$\frac{3}{2}^-$	→	$\frac{1}{2}^-$	9 ± 3	6.6
	15.06	→	0	$\frac{3}{2}^-;\frac{3}{2}$	→	$\frac{1}{2}^-;\frac{1}{2}$	0.51 ± 0.18	1.14
^{14}C	7.01	→	0	2^+	→	0^+	3.6 ± 0.6	9.17
^{14}N	3.95	→	0	1^+	→	1^+	3.6 ± 0.2	5.56
	7.03	→	0	2^+	→	1^+	3.0 ± 0.8	2.96
		→	2.31		→	$0^+;1$	0.32 ± 0.08	0.44
	9.17	→	2.31	$2^+;1$	→	$0^+;1$	5.0 ± 0.6	3.66
		→	7.03		→	$2^+;0$	8.6 ± 5.4	0.350
^{15}N	6.32	→	0	$\frac{3}{2}^-$	→	$\frac{1}{2}^-$	6.4 ± 0.53	8.06

[a] T shown in usual convention $[J^\pi;T]$ only if transitions from the initial state involve a change in T.
[b] The experimental data is taken from refs. [26-28] and [35].

and B(M1) and B(E2) transition strengths quite well. The wave functions are now used to calculate log ft values for allowed β decays. We have carried out an investigation of Fermi and Gamow-Teller types of allowed β decay.

The theoretical log ft values for the transitions between the ground states and low-lying levels for $A = 6$–15, obtained with the wave functions from the PTBME interaction, are compared in Table 13 to their experimental counterparts taken from refs. [25] to [28] and [45]. The

6.2 Gamow-Teller strength distributions

A sensitive test of the wave functions is provided by comparing the total theoretical Gamow-Teller strength and its distribution over the energy levels in the final nucleus to experimental data. This stems from the fact that the Gamow-Teller operator only acts on the intrinsic quantum numbers of the nucleon i.e., spin and isospin, without affecting the spatial configurations.

Beta decay alone cannot be used to extract information on Gamow-Teller transition strengths because of the strict limit imposed by the energetics of the reaction: Denoting the mass of the parent nucleus by M_P and that of the daughter by M_D, β^- decay can only proceed if $M_{P(Z)} > M_{D(Z+1)}$ is satisfied, and β^+ decay if $M_{P(Z)} > M_{D(Z-1)} + 2m_e$ is satisfied (m_e is the mass of the electron). Much of the available experimental data is thus provided by (p,n) and (n,p) reactions at excitation energies up to several MeV since these lead to transitions that are analogous to Gamow-Teller and Fermi β decay.

We have carried out an investigation of the distribution of the Gamow-Teller strengths over all the states allowed in the final nucleus. The theoretical Gamow-Teller transition strengths, determined with the p–shell wave functions obtained with the PTBME interaction, are plotted (inverted plots) in Figures 14 to 24 as a function of the (theoretical) excitation energy in the final nucleus. Only transitions from the ground state of the initial nucleus with $A = 6 - 14$ were considered. The experimental Gamow-Teller transition strengths available, taken from refs. [47] to [49], are also plotted (upright plots) against the experimental excitation energies. The experimental uncertainty in the absolute cross-sections has been estimated to be about 13% [48].

The ^{6}Li $\rightarrow$ ^{6}Be transitions. Almost all of the Gamow-Teller transition strength is concentrated in the transition to the ground state of ^{6}Be. The experimental Gamow-Teller strength is about 80% of the theoretical value predicted with the wave functions of the PTBME interaction.

The ^{7}Li $\rightarrow$ ^{7}Be transitions. The distribution plot shows that most of the Gamow-Teller strength is concentrated in the transition to the $\frac{3}{2}^-$ ground state and first $\frac{1}{2}^-$ excited state at the (theoretical) excitation energy of about 0.85 MeV. Small but measurable amounts of strengths is also found for the transitions to states with theoretical excitation energies around 7 to 14 MeV. The total observed strength is about 87% of the theoretical value.

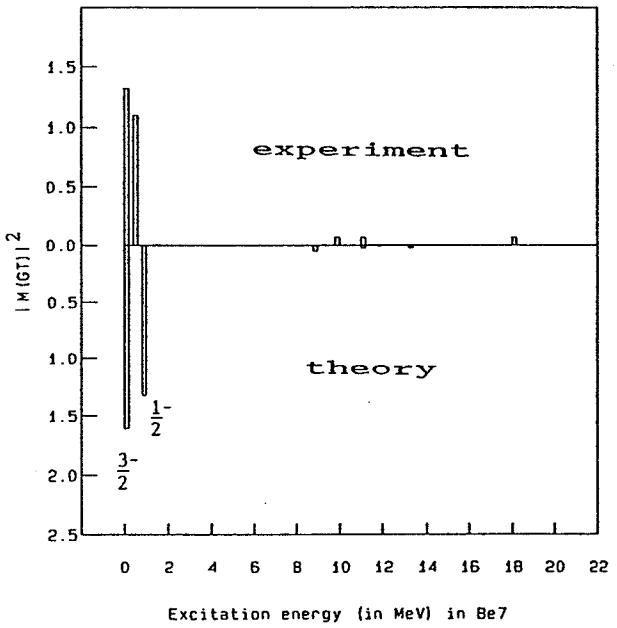

Figure 15 Gamow-Teller strength distribution in the transition of ^{7}Li to ^{7}Be.

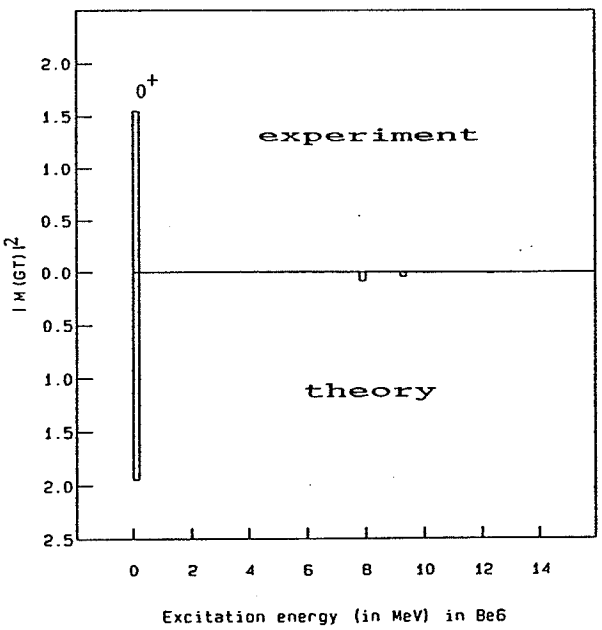

Figure 14 Gamow-Teller strength distribution in the transition of ^{6}Li to ^{6}Be.

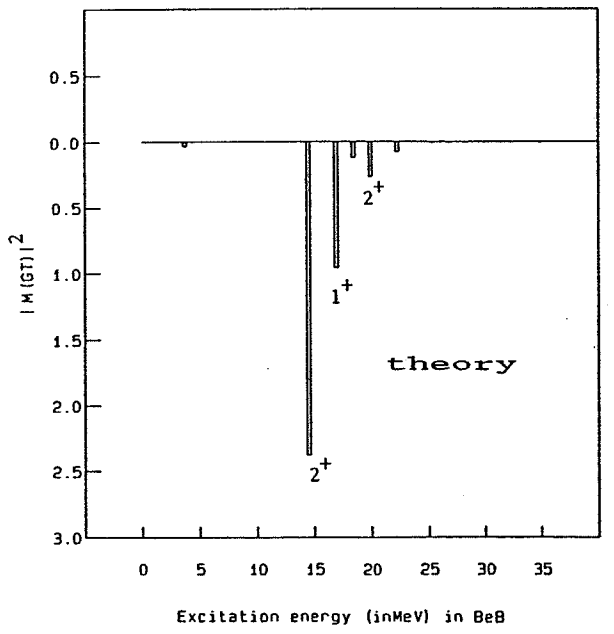

Figure 16 Gamow-Teller strength distribution in the transition of ^{8}Li to ^{8}Be.

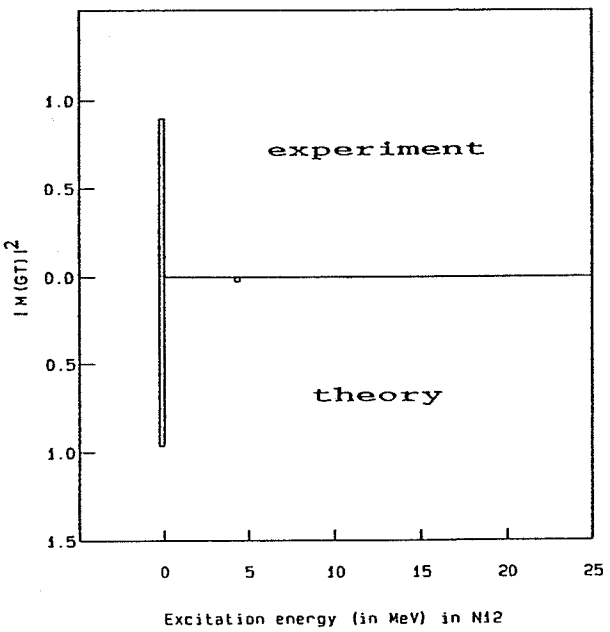

Figure 21 Gamow-Teller strength distribution in the transition of ^{12}C to ^{12}N.

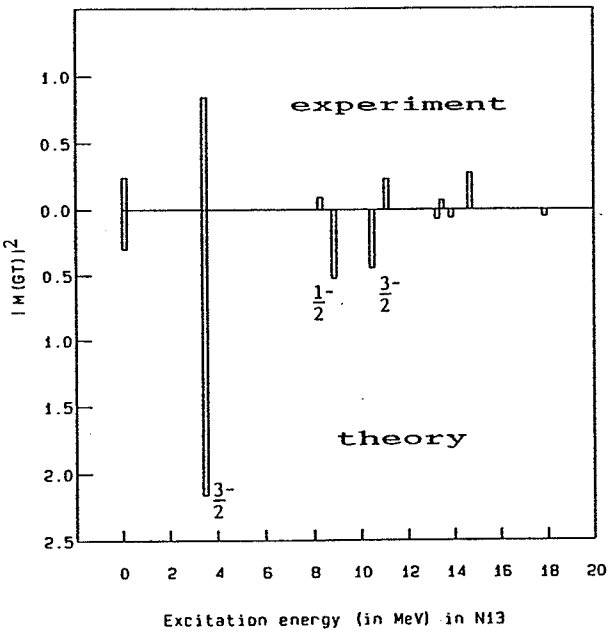

Figure 23 Gamow-Teller strength distribution in the transition of ^{13}C to ^{13}N.

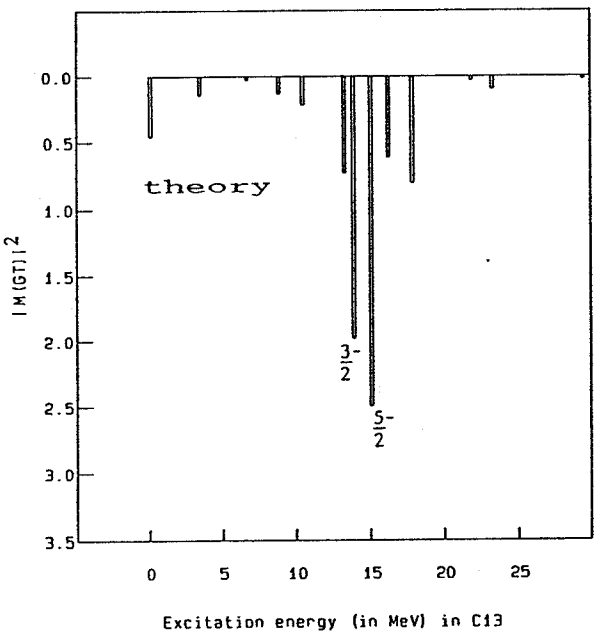

Figure 22 Gamow-Teller strength distribution in the transition of ^{13}B to ^{13}C.

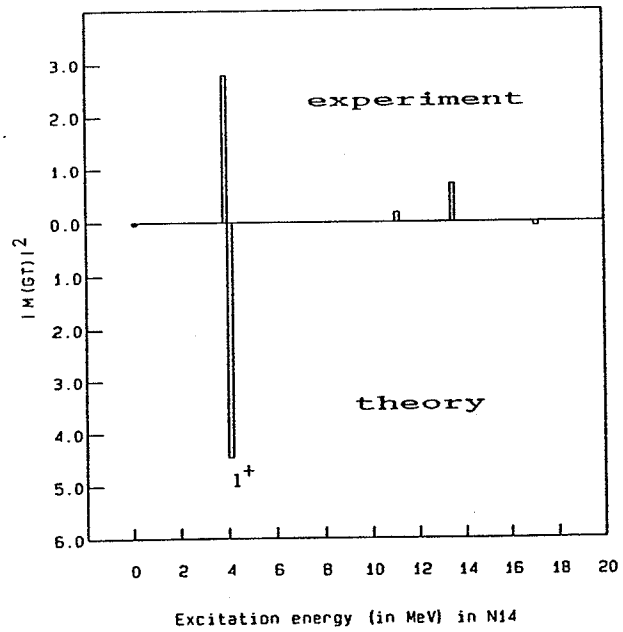

Figure 24 Gamow-Teller strength distribution in the transition of ^{14}C to ^{14}N.

tion of Cohen and Kurath. For the total Gamow-Teller transition strength we obtain a value of 3.115. This should be compared with the experimental value [49] of $\sum |M(\mathrm{GT})|^2 \approx 2.2$, which is about 70% of the PTBME and Cohen and Kurath values, using the 2BME(6–16) interaction.

The ^{10}Be $\rightarrow$ ^{10}B transition. Note that the first $1^+,0$ and $3^+,0$ (ground state) levels for ^{10}B are virtually degenerate for PTBME (see Fig. 7). No Gamow-Teller transition occurs to the ground state in ^{10}B. Almost all of the Gamow-Teller transition strength is contained in the transitions to the first two $1^+;0$ levels in the daughter nucleus, with the second carrying about 15% of the total. The wave function obtained with the PTBME interaction predicts a value of 3.0 for the total Gamow-Teller transition strength. Small contributions to the Gamow-Teller strength are found at (theoretical) excitation energies around 10 MeV.

The ^{11}B $\rightarrow$ ^{11}C transitions. The theoretical Gamow-Teller strength is mostly concentrated in the transitions to the lowest two $\frac{3}{2}^-$, $\frac{5}{2}^-$ states and the lowest $\frac{1}{2}^-$ state in ^{11}C. The total sum obtained for the experimental

[21] H.U. Jäger and M. Kirchbach, Nucl. Phys. A **291** (1977) 52.

[22] D.J. Millener and D. Kurath, Nucl. Phys. A **255** (1975) 315.

[23] W.D. Teeters and D. Kurath, Nucl. Phys. A **275** (1977) 61.

[24] B.A. Brown, W.A. Richter, R.E. Julies and B.H. Wildenthal, Ann. of Phys. **182** (1988) 191.

[25] Table of Isotopes ed. Michael Lederer and Virginia S. Shirley, 7th edition, Wiley, New York, 1978.

[26] F.Ajzenberg-Selove, Nucl. Phys. A **490** (1988) 1.

[27] F.Ajzenberg-Selove, Nucl. Phys. A **506** (1990) 1.

[28] F.Ajzenberg-Selove, Nucl. Phys. A **449** (1986) 1.

[29] F.Ajzenberg-Selove, Nucl. Phys. A **460** (1986) 1.

[30] P.J. Brussaard and P.W.M. Glaudemans, "Shell Model Applications in Nuclear Spectroscopy", North-Holland, Amsterdam, 1977.

[31] A.H. Wapstra and G. Audi, Nucl. Phys. A **432** (1985) 1.

[32] A. Hosaka, K.I. Kubo and H. Toki, Nucl. Phys. A **44** (1985) 76. Note the following corrections: in Eq.(2) σ should be replaced by s, in Eq. (3) the $Y_{LS}(x)$ term should have a factor $\frac{e^{-x}}{x^2}$ in place of $\frac{e^{-x}}{x}$, and in Table 3 the range should be 0.40 rather than 0.50.

[33] W.A. Richter, M.G. van der Merwe, R.E. Julies and B.A. Brown, Nucl. Phys. A **523** (1991) 325.

[34] D. Mikolas, B.A. Brown, W. Benenson, L.H. Harwood, E. Kashy, J.A. Nolen, Jr., B. Sherrill, J. Stevenson, J. S. Winfield and Z. Q. Xie, Phys. Rev. C **37** (1988) 766.

[35] P.M. Endt, At. Data and Nucl. Data Tables **23** (1979) 3.

[36] E.K. Warburton, J.W. Olness, S.D. Bloom and A.R. Poletti, Phys. Rev. **171** (1968) 1178.

[37] B.N. Taylor, W.J. Parker and D.N. Langenberg, Rev. Mod. Phys. **41** (1969) 375.

[38] D.H. Wilkinson, Nucl. Phys. A **209** (1973) 470.

[39] D.H. Wilkinson and B.E.F. Macefield, Nucl. Phys. A **232** (1974) 58.

[40] A. Kropf and H. Paul, Z. Phys. **267** (1974) 129.

[41] S. Raman, T.A. Walkiewicz and H. Behrens, Nucl. Data Sheets **16** (1975) 451.

[42] J.C. Hardy and I.S. Towner, Nucl. Phys. A **254** (1975) 221.

[43] V.E. Krohn and G.R. Ringo, Phys. Lett. B **55** (1975) 175.

[44] D.H. Wilkinson, Nucl. Phys. A **377** (1982) 474.

[45] F. Ajzenberg-Selove, Nucl. Phys. A **310** (1979) 1.

[46] H.J. Rose O. Häusser and E.K. Warburton, Rev. Mod. Phys. **40** (1968) 591.

[47] T.N. Taddeucci, J. Rapaport, D.E. Bainum, C.D. Goodman, C.C. Foster, C. Gaarde, J. Larsen, C.A. Goulding, D.J. Horen, T. Masterson, E. Sugerbaker, Phys. Rev. C **25** (1981) 1094.

[48] T.N. Taddeucci, C.A. Goulding, T.A. Carey, R.C. Byrd, C.D. Goodman, C. Gaarde, J. Larsen, D. Horen, J. Rapaport, E. Sugerbaker, Nucl. Phys. A **469** (1987) 125.

[49] J. Rapaport, Can. J. of Phys. **65**, (1987) 574.

[50] A. Weller, P. Egelfof, R. Čaplar, O. Karban, D. Krämer, K.H. Möbius, Z. Moroz, K. Rusek, E. Steffens, G. Tungate, K. Blatt, Ilse Koenig and D. Fick, Phys. Rev. Lett. **55** (1985) 480.